Ferroelectrics

ISSN: 0015-0193 (Print) 1563-5112 (Online) Journal homepage: https://www.tandfonline.com/loi/gfer20

Application of thin film barium strontium titanate (BST) in a microcontroller based tool to measure oxygen saturation in blood

Johan Iskandar, Renan Prasta Jenie, Ulfah Juniarti Siregar, Brian Yuliarto & Irzaman

To cite this article: Johan Iskandar, Renan Prasta Jenie, Ulfah Juniarti Siregar, Brian Yuliarto & Irzaman (2020) Application of thin film barium strontium titanate (BST) in a microcontroller based tool to measure oxygen saturation in blood, Ferroelectrics, 554:1, 134-143, DOI: 10.1080/00150193.2019.1684755

To link to this article: https://doi.org/10.1080/00150193.2019.1684755

Published online: 25 Feb 2020.

FERROELECTRICS
2020, VOL. 554, 134–143
https://doi.org/10.1080/00150193.2019.1684755

Taylor & Francis
Taylor & Francis Group

Application of thin film barium strontium titanate (BST) in a microcontroller based tool to measure oxygen saturation in blood

Johan Iskandar[a,b], Renan Prasta Jenie[c,d], Ulfah Juniarti Siregar[e], Brian Yuliarto[f], and Irzaman[g,h]

[a]Department of Computer Technology, Vocational School, Universitas Pakuan, Bogor, Indonesia; [b]Alumnus of Department of Physics, Faculty of Mathematics and Natural Sciences, IPB University, Bogor, Indonesia; [c]Department of Community Health, Faculty of Community Health, Universitas Binawan, Jakarta, Indonesia; [d]Alumnus of Department of Community Nutrition, Faculty of Human Ecology, IPB University, Bogor, Indonesia; [e]Department of Silviculture, Faculty of Forestry, IPB University, Bogor, Indonesia; [f]Advanced Functional Materials Laboratory, Department of Engineering Physics, Faculty of Industrial Technology, Institut Teknologi Bandung, Bandung, Indonesia; [g]Department of Physics, Faculty of Mathematics and Natural Sciences, IPB University, Bogor, Indonesia; [h]Researcher of Surfactant and Bioenergy Research Center (SBRC) of the Institute for Research and Community Service (LPPM IPB), IPB University, Bogor, Indonesia

ABSTRACT

Tools to measure pulse and blood SpO_2 have been made using thin-film barium strontium titanate (BST) as the sensor. There are three phases in designing a prototype for measuring the pulse and SpO_2. The first is constructing and profiling the optical and electrical characteristics of thin-film BST. From the optical characteristic profiling, it was discovered that there are three wave peaks that are absorbed the most by the film: 450, 600–640, and 900 nm. From the electrical characteristic profiling, it was discovered that the film produced is classified as a photodiode with two sensitivities: exp(–0.0018)/lux when illuminated by white light and exp(–0.0429)/lux when illuminated by infrared light. The second is designing the electronic circuit which consists of an amplifier circuit, filter, and a minimum Atmega328P-PU microcontroller system. From the tests that had been conducted, each circuit succeeded in processing the signal as expected. The third, testing the SpO_2 on 20 patients using the prototype and a standard model Elitech Fox-1 oximeter as the reference tool. The results that were recorded demonstrated that the accuracy of the prototype in measuring the SpO_2 reached 98% in comparison to the reference tool.

ARTICLE HISTORY
Received 16 May 2019
Accepted 5 September 2019

KEYWORDS
Barium strontium titanate; microcontroller; optical properties; oxygen saturation; photodiode

1. Introduction

Ferroelectric materials are currently being developed for various purposes, especially as part of microelectronic devices. Ferroelectric materials that are made into thin films can be utilized as a switch, light detector, and automatic devices that use the optical principle in their working system.

CONTACT Johan Iskandar johan_iskandar@rocketmail.com Department of Computer Technology, Universitas Pakuan, 16143 Bogor, Indonesia; Irzaman irzaman@apps.ipb.ac.id Department of Physics, Faculty of Mathematics and Natural Sciences, IPB University, 16680 Bogor, Indonesia.

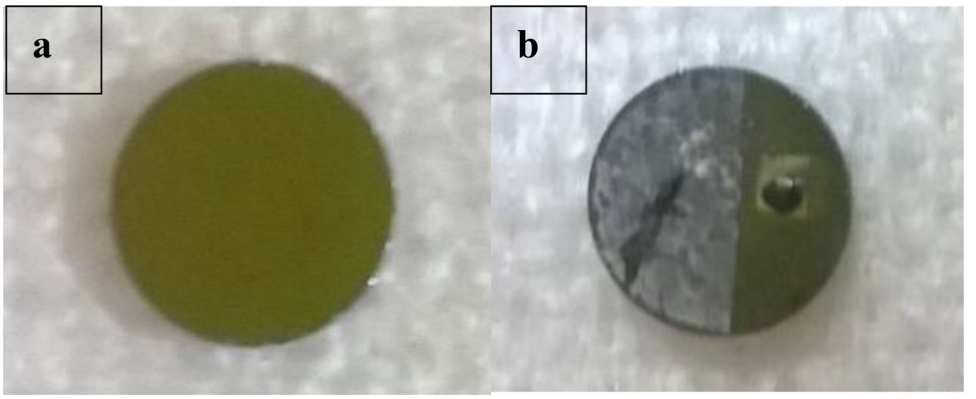

Figure 1. Silicon substrate (a), BST on Si(100) (b).

Ferroelectric materials consist of complex chemical compounds and up to this day there are nearly 100 inorganic compounds; simple compounds such as NH_4HSO_4 (monoclinic), KH_2PO_4 (orthorhombic), and $BaTiO_3$ (tetragonal) [1–3]. In this study, the ferroelectric material barium strontium titanate was used as a thin film on the Si(100) substrate with the film synthesis method using the chemical solutions deposition (CSD) method assisted by the spin-coating technique [4,5].

Currently, strontium titanate-doped barium titanate is very useful in industries because of its versatility. A number of barium strontium titanate (BST) applications are as dynamic random access memory capacitors, microwave filters, infrared detectors, and dielectric phase shifters [6–8]. BST is a complex oxide which consists of a solid solution of barium titanate $BaTiO_3$ (BT) which is a ferroelectric material with a Curie temperature of 130 °C and strontium titanate $SrTiO_3$ (ST) which at room temperature is a paraelectric material [9–11]. Barium titanate and strontium titanate have an ABO_3 perovskite structure (where A = Ca, Sr, La; B = Nb, Ta, Zr) and are excellent as a raw material for making a film [5,12–14].

2. Methods

We have separated a solution of substrates and La dopant in three dopant groups (0%, 5%, and 10%). The substrate used was type-p Si(100). The substrate was cut into a circle with a diameter of 8 mm (Figure 1a) then rinsed by immersion in distilled water for 5 min [10,13]. The BST solution was made by reacting [$Ba(CH_3COO)_2$, 99%], [$Sr(CH_3COO)_2$, 99%], and [Ti ($C_{12}O_4H_{28}$), 97.999%] in 2.5 ml [$H_3COOCH_2CH_2OH$, 99%] as the solvent in a test tube while being vibrated ultrasonically. The reaction equation for the formation of the BST solution is as follows [15–18].

Coating of the BST solution of a third of the substrate surface (Figure 1b) was conducted using the CSD method assisted by the spin-coating technique at a speed of 3000 rpm, repeated triplicate. The next step was annealing at 850 °C for 22 h and the contact installation. The last step was an assessment of the optical properties to determine the energy band gap and refraction index, electrical properties which includes current-voltage (I-V) and sensitivity, XRD characterization was done to assess lattice parameter of BST thin films, and FTIR spectroscopy was done to determine molecular

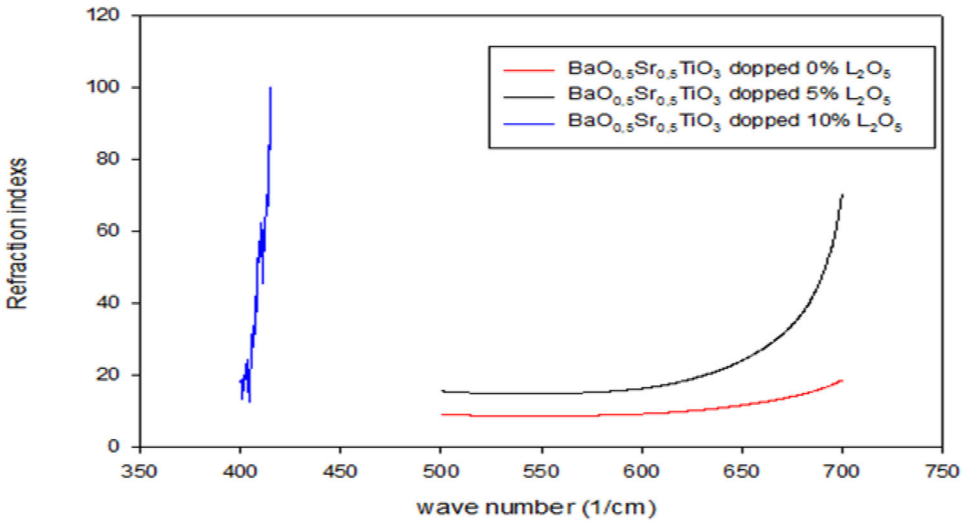

Figure 2. Refractive index.

functional group or compound analysis. PSA was done to determine the particle size and distribution of BST thin films samples.

The BST film produced was then applied in an electronic circuit as a light sensor for detecting oxygen saturation in blood.

The source of voltage (Vcc) used was 5 V. For each circuit, measurements of the output voltage and frequency (f) were taken and then compared with the analytic calculation results. Measurement accuracy was calculated using the following equation:

$$accuracy = \left[1 - \left|\frac{h - x}{h}\right|\right] \times 100\%, \tag{1}$$

where x is the average measurement data and h is the expected value.

3. Results and discussion

3.1. The thin-film BST synthesis and characterization

Optical test shows increase in the refractive index while increasing the number of Lanthanum dopant La_2O_3. Very significant improvement occurred in BST doped Lanthanum 10%, due to the polarity and irregularities in the layer structure. Addition of La dopant increases the refractive index. Increase in the refractive index (Figure 2) means much harder light conductivity through a medium. If it used as a sensor, it would have lower sensitivity level.

We have proven that La dopant addition could increase band gap energy. In theory, the presence of impurities makes energy level of band gap conduction narrower with the valence band means energy band gap is getting small [19]. However, our result (Figure 3) shows otherwise dopant increases the energy band gap. High energy gap means more difficult electrons movement in semiconductors, means that the materials quality as a sensor decreases. This results in agreement with [13]. Ba and Sr atoms variance in BST thin layer surface may cause energy band gap increase.

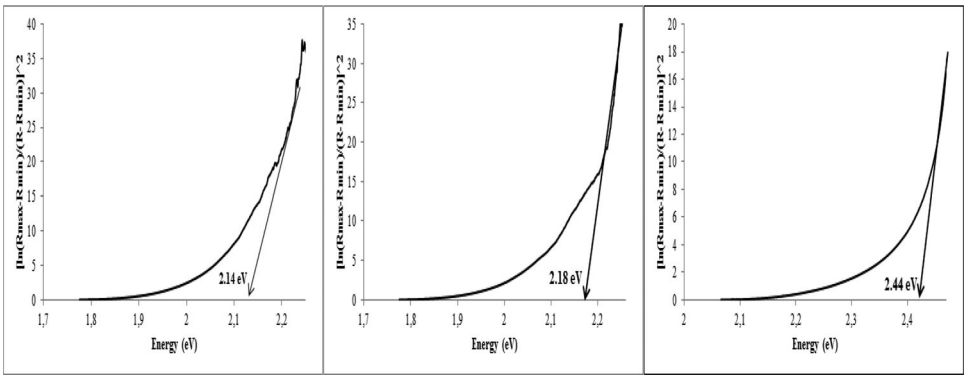

Figure 3. Addition of Lanthanum dopant (a) 0%, (b) 5%, (c) 10% increases BST energy gap. The results are consistent with the Si energy gap.

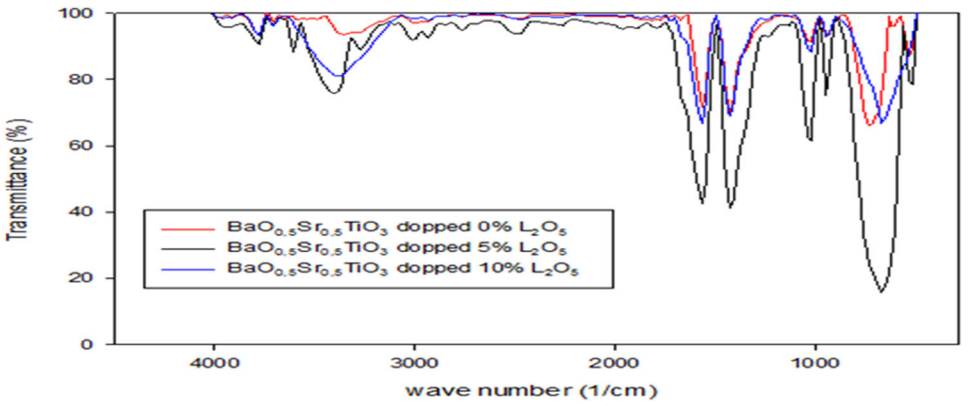

Figure 4. Residual water and hydroxyl groups detected in the sample.

We have proven that addition of La dopant increases particle size (Figure 4). The most massive particle size shown by 10% La dopant BST, with a particle size between 700 and 800 nm.

Residual water and hydroxyl groups detected in the sample. Absorption at 2720, 2761, and 2454 cm^{-1} shows methyl CH3 weak bond. Absorption at 1759 cm^{-1} shows weak bond ester C=O stretching. Absorption at 1420–1558 cm^{-1} provides a strong CO vibration. Absorption at 509 cm^{-1} and 663 cm^{-1} shows deformation mode. The 5% LT dopant BST has shown highest absorption (Figure 5).

Addition of La dopant lowering c/a lattice parameter. La dopant introduces small changes to BST film lattice parameters (Figure 6). The crystal structure is tetragonal (Table 1). The crystal structure is in agreement with [4], in which the crystal structure should be octahedral inside a tetragonal. Our conjecture, the La dopant replacing some Ba in BST, creating n-type BST film, because Ba covalent radius (1.49 Å) is closer to La (1.69 Å) than Sr (1.32 Å) and Ti (0.745 Å).

3.2. Circuit design and integration of BST film

The BST film used in the prototype was decided based on the results of testing the optical properties and structure properties (XRD and FTIR). Based on the results of

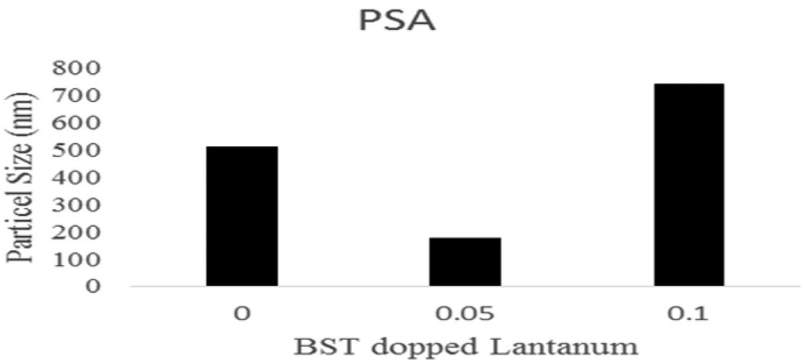

Figure 5. Particle size analysis of BST doped lanthanum by 0%, 5%, and 10%.

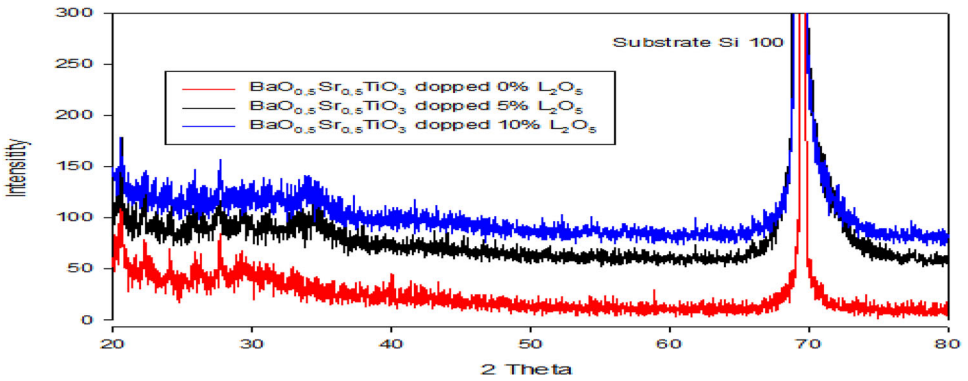

Figure 6. Lanthanum dopant introduces small changes to BST film lattice parameters.

Table 1. Addition of lanthanum dopant lowering c/a lattice parameter.

	Si (100)			
Dopant	*a* (Ao)	*c* (Ao)	*c/a*	Grand size (Ao)
0%	3.9707	4.00916	1.00969	513
5%	3.96949	3.97993	1.00263	177.88
10%	3.97972	3.98705	1.00184	741.51

The crystal structure is tetragonal.

testing the optical properties are highly considered the value of the energy gap. The smaller the energy gap film, the easier it is for electrons to move from the valence band to the conduction band. In this case, BST is chosen without doping (0%) because it has the smallest energy gap with a value of 2.14 eV compared to a 5% doping BST (2.18 eV) and 10% (2.44 eV). Whereas seen from the lattice parameter, the value of the c/a ratio chosen is the biggest because it has the highest dipole moment and spontaneous polarization. From Table 1, the highest c/a ratio is BST with 0% doping. With this claim, the BST film used as a sensor in the prototype is a 0% doping BST film.

Sensor BST with 0% doping needs I-V testing to find out whether it is able to distinguish changes in light intensity through shifting the I-V curve. The I-V testing results (Figure 7a) revealed that thin-film BST was sensitive to light because there was a shift in the I-V curve from light to dark conditions with the characteristics of a photodiode

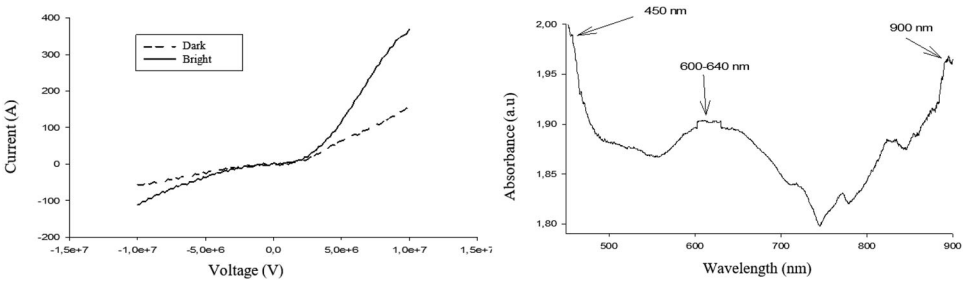

Figure 7. (a) The shift in the thin-film BST I-V curve from dark to bright conditions and (b) thin-film BST absorbance curve.

curve. The curve shift occurred because the electrons in the film flowed more easily when receiving light and it became more conductive [13].

The I-V curve only provides information about the film's sensitivity to incoming light; therefore, testing of the optical characteristics needed to be conducted in order to obtain a more specific wavelength which could be responded well by the film. Figure 7b is the results of the absorbance testing using an ocean optics DT-mini 2 model Vis-NIR spectrophotometer. The absorbance curve obtained revealed that the thin-film BST absorbed more of the blue (450 nm), orange–red (600–640 nm), and Near Infrared (NIR) (900 nm) light according to the curve peak. The absorbance curve peaks mean that the film is very sensitive in responding to the wavelengths at those points. This value was suitable for application in this study because it matched the character of the LED used (640 and 910–940 nm).

The I-V testing had shown that thin-film BST is sensitive to light, but the data did not provide sufficient information on how sensitive the film is to changes in the intensity of the light that strikes it. Therefore, a sensitivity test was conducted by varying the intensities of white light and NIR light. The sensitivity of the BST film showed the amount of change in the resistance when there was a change in light intensity of 1 lux [20]. Figure 8 is the thin-film BST sensitivity curve obtained from the data plot of resistance change against the intensity change. The film was very sensitive to a range of 1000–2000 lux when illuminated with white light and 10–40 lux when illuminated with NIR. Based on the absorbance curve, even though more NIR was absorbed by the film than white light, but the white light's photon energy was greater than that of NIR. Therefore, the slope of the sensitivity curve when illuminated with white light was greater than when illuminated with NIR. Photon energy had a great influence on the change in film's resistance change. The greater the photon energy, the smaller the film BST resistance is, or in other words the electrons had enough energy to exit from the valence band to the conduction band and cause the current flowing to become larger.

The change in signal voltage by thin-film BST was still very small with a value less than the minimum value for the signal to be able to be read by the microcontroller; therefore, an amplifying circuit was required. Figure 9 is a cascade amplifying circuit with three amplifying steps. The first step was to amplify the signal voltage by 39 gains from the film which had been assembled with a Wheatstone bridge.

The testing of the amplifying circuit for measuring SpO_2 used AC and DC voltage sources. The curves in Figure 10a,b revealed a difference in the experiment's output voltage result and that of the analytical calculations (ideal value). The optimum DC

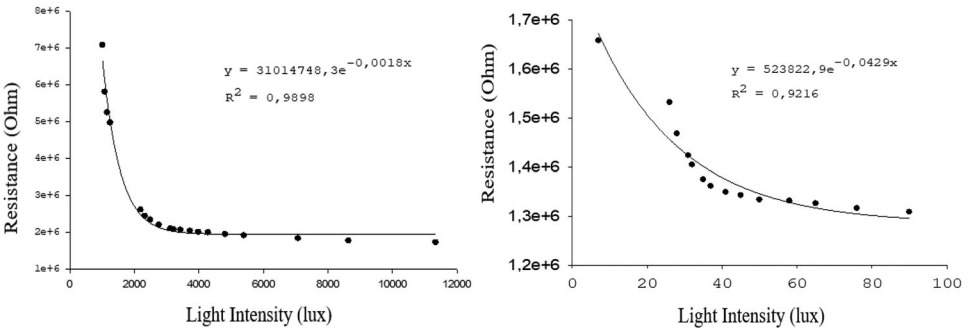

Figure 8. (a) Thin-film BST's sensitivity to white and (b) NIR.

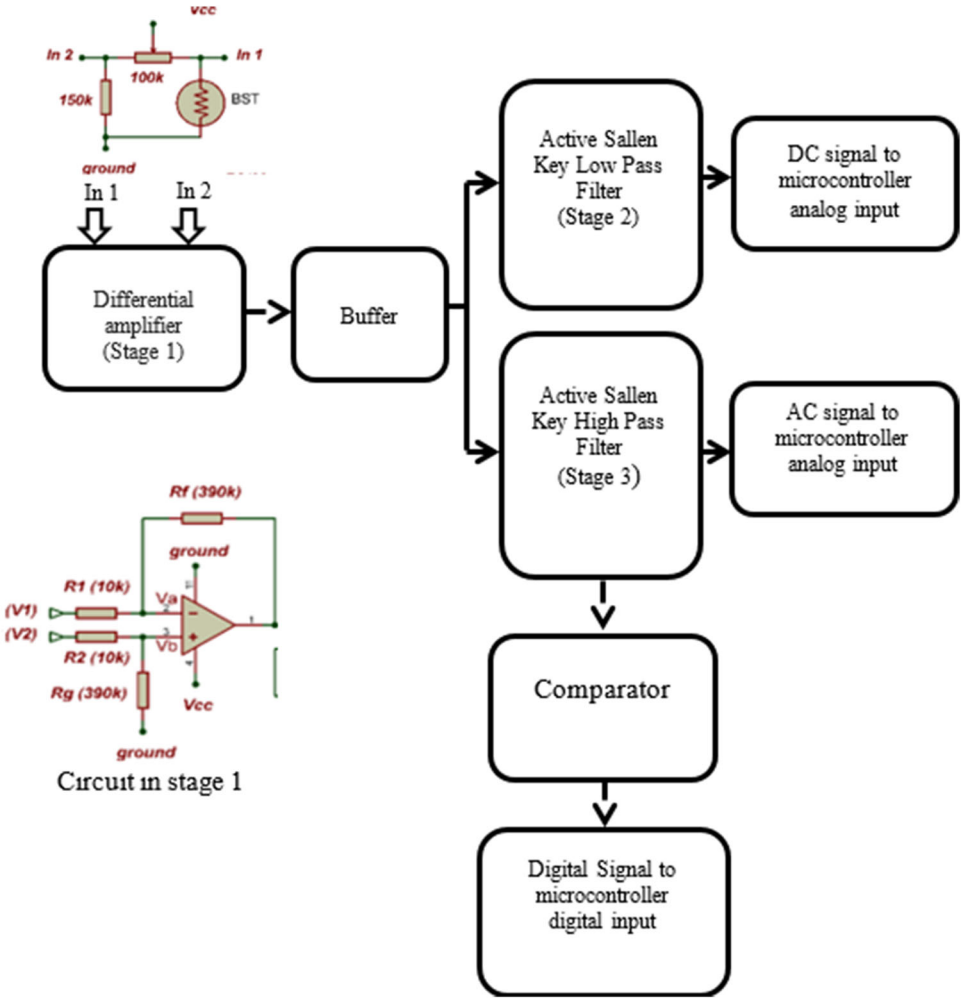

Figure 9. The cascade amplifying circuit scheme for measuring SpO_2.

voltage that could be amplified by the circuit was 0.103 V with an output voltage of 3.46 V, while the optimum AC input voltage was 0.108 V with an output voltage of 0.475 V. The differences between the results of the experiment and the analytical results

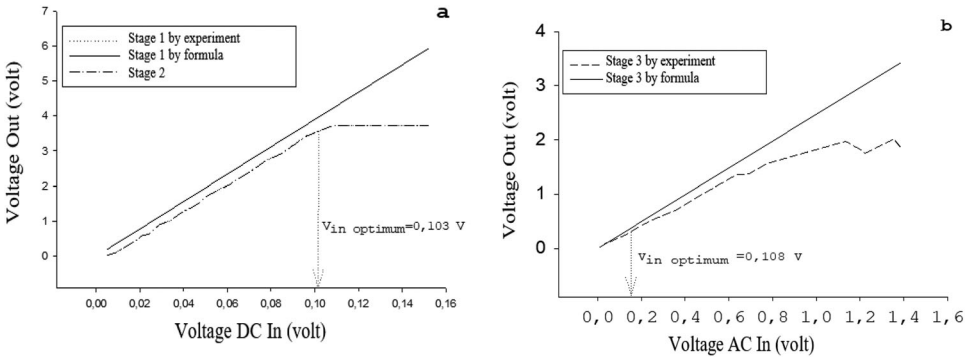

Figure 10. The amplifying circuit's response in the SpO2 measurement of the DC (a) and (b) AC voltage.

were believed to be influenced by the power loss in IC TL074CN. This was supported by the decreased voltage in IC TL074CN which was only 4.84 V while it should have been 5 V.

In order to know whether the filter circuit functioned well, observations were made by providing a voltage from the signal generator, and then the output signal was measured using an oscilloscope. The signal that succeeded in passing was analyzed using Equation (2) to determine the frequency. Figure 11a shows that the circuit in step two was able to allow the DC voltage signal with a frequency below f_{cLPF} which was 0.13 Hz to pass through and in step three it could allow the AC voltage signal above f_{cHPF} which was 1.02 Hz to pass through:

$$f = \frac{n}{t_n}, \tag{2}$$

where n is the number of waves and t_n is the time in seconds.

3.3. Prototype testing

The accuracy and confidence level of the measurements taken by the prototype made was strongly influenced by the suitability with the wavelength of the LED light used. Therefore, the testing on LEDs was conducted using a Vis-NIR spectrophotometer from the wavelength range of 450–1000 nm. The test results in Figure 11b revealed that the LED wavelength was suitable with the absorbed wavelength from oxyhemoglobin and deoxyhemoglobin.

The SpO_2 measurement process by the prototype was conducted in two main steps. The first step was turning on the red and infrared LED in turns for 5 s which was controlled by the microcontroller. During the first 5 s, the red LED was on and the infrared LED was off so that the DC and AC voltage signals in the amplifying circuit only came from the red LED. During the next 5 s, the infrared LED was on and the red LED off so that the DC and AC voltage signals in the circuit only came from the infrared LED. The voltage signal which exited the amplifying circuit was an analog signal; therefore, it could be processed by the microcontroller without having to be altered into a digital signal by the analog to digital converter feature in the microcontroller. The second step

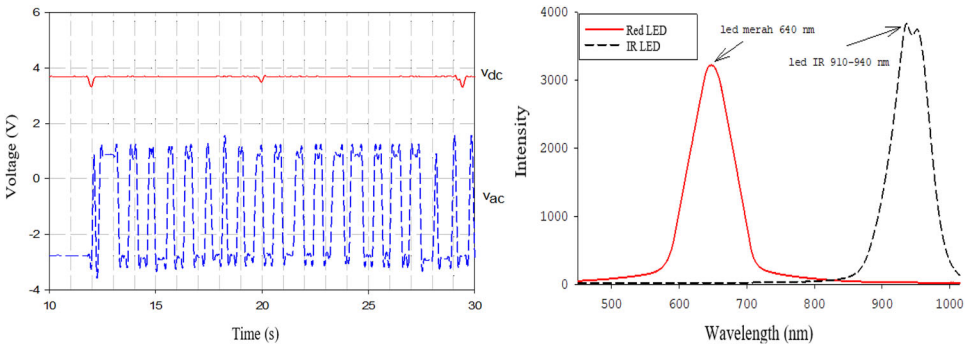

Figure 11. (a) Circuit testing results for the SpO_2 measurements on direct current (vdc). (b) The red and infrared LED spectrums used in the prototype.

was a follow up on the digital signal which was the conversion result of the analog signal. The digital signal that was stored was processed by the microcontroller according to Equations (3) and (4) to obtain the SpO_2 percentage in the blood and the results were displayed on a 16×2 character LCD:

$$r = \frac{V_{AC\ red}/V_{DC\ red}}{V_{AC\ IR}/V_{DC\ IR}}, \tag{3}$$

$$SpO_2 = 100\% \times r. \tag{4}$$

To guarantee that the percentage of oxygen saturation measured was from a human being, the prototype conducted an initial scanning of the heart rate. If the results of the scanning revealed minor results (no pulse or the absence of a pulse outside the human heart rate range), the prototype would not conduct an SpO_2 reading.

Testing of the prototype was conducted on 20 patients. The measurement results were not much different from the measurements taken by a standard oximeter. This was seen from the average accuracy value that reached 98%. Even though the average accuracy was quite high, quite a lot of the data was not in line with the standard oximeter, and this was due to a number of main factors, namely effects of external light and the instability of the finger position during the reading. In these conditions, the changes of the signal read by the sensor were not solely from the specific LED used, but were influenced by those factors.

4. Conclusion

By exploiting optical and electrical properties, thin-film BST could be used as a sensor in a measurement tool for oxygen saturation in blood.

Funding

We gratefully acknowledge the funding from the Kementerian Riset, Teknologi dan Pendidikan Tinggi, Republic of Indonesia grant 2019, and we also gratefully acknowledge the funding from United States Agency for International Development through Sustainable Higher Education Research Alliances program Center for Development of Sustainable Region (CDSR) 2018.

References

[1] A. W. Nuayi *et al.*, Enhancement of photon absorption on Ba_x $Sr_{1-x}TiO_3$ thin-film semiconductor using photonic crystal, *Int. J. Optics*. **2014**, 1 (2014). DOI: 10.1155/2014/534145.

[2] K. Neeraj and R. Nath, Ferroelectric properties of potassium nitrate-polymer composite films, *J. Pure Appl. Ind. Phys*. **1**, 21 (2014).

[3] D. V. Stryukov *et al.*, Specific features of the ferroelectric state in two-layer barium strontium titanate-based heterostructures, *J. Phys. Solid State*. **60** (1), 115 (2018). DOI: 10.1134/S1063783418010250.

[4] A. E. Souza *et al.*, Morphological and structural changes of $Ca_xSr_{1-x}TiO_3$ powders obtained by the microwave-assisted hydrothermal method, *Int. J. Appl. Ceram. Technol*. **9**, 189 (2011). DOI: 10.1111/j.1744-7402.2011.02648.x.

[5] M. Willander *et al.*, Determination of A.C. conductivity of nano-composite perovskite $Ba_{(1-x-y)}Sr_{(x)}O_3$ prepared by sol-gel technique, *J. Cryst. Proc. Technol*. **02** (01), 1 (2012).

[6] F. Mao-Yan Sheng-Lin, Influence of La-Mn-Al co-doping on dielectric properties and structure of BST thick film, *J. Elect. Sci. Technol. China*. **7**, 281 (2009).

[7] V. S. Puli *et al.*, Nanoscale ferroelectric switchable polarization and leakage current behavior in $(Ba_{0.50}Sr_{0.50})(Ti_{0.80}Sn_{0.20})O_3$ thin films prepared using chemical solution deposition, *J. Nanomater*. **2015**, 1 (2015). DOI: 10.1155/2015/340616.

[8] S. K. Barik, R. N. P. Choudhary, and A. K. Singh, AC impedance spectroscopy and conductivity studies of $Ba_{0,8}Sr_{0,2}TiO_3$ ceramics, *J. Adv. Mater. Lett*. **2**, 419 (2011). DOI: 10.5185/amlett.2011.2228.

[9] A. A. Saif, N. Ramli, and P. Poopalan, AFM study of multilayer sol-gel $Ba_xSr_{1-x}TiO_3$ thin films, *J. Jordan Phys*. **3**, 62 (2010).

[10] S. A. Muravov *et al.*, The study of ferroelectric thin films on silicon substrates, *J. Meas. Eng*. **1**, 25 (2013).

[11] B. Ertug, The overview of the electrical properties of barium titanate, *Am. J. Eng. Res*. **2**, 7 (2013).

[12] Irzaman *et al.*, The effect of Ba/Sr ratio on electrical and optical properties of Ba_x $Sr_{(1-x)}$ TiO_3 (x = 0.25; 0.35; 0.45; 0.55) thin film semiconductor. *J. Ferroelect*. **445**, 11 (2013).

[13] J. Iskandar *et al.*, Characterization of electrical and optical properties on ferroelectric photodiode of barium strontium titanate ($Ba_{0.5}Sr_{0.5}TiO_3$) films based on the annealing time differences and its development as light sensor on satellite technology, *Proc. Environ. Sci*. **24**, 326 (2015).

[14] Irzaman *et al.*, Surface roughness and gain size characterization of effect of annealing temperature for growth gallium and tantalum doped $Ba_{0,5}Sr0_{,5}TiO_3$ thin film. *J. Atom Indonesia*. **35**, 60 (2009). DOI: 10.17146/aij.2009.48.

[15] A. V. Tumarkin and A. A. Odinets, Domain epitaxial growth of ferroelectrics films of barium strontium titanate on sapphire, *Phys. Solid State*. **60** (1), 87 (2018). DOI: 10.1134/S1063783418010274.

[16] Irzaman *et al.*, Application of lithium tantalite ($LiTaO_3$) films as light sensor to monitor the light status in the Arduino Uno based energy-saving automatic light prototype and passive infrared sensor, *J. Ferroelect*. **524**, 46 (2018).

[17] Irzaman *et al.*, Characterization of $Ba_{0.55}Sr_{0.45}TiO_3$ films as light and temperature sensors and its implementation on automatic drying system model, *J. Integrated Ferroelect*. **168**, 137 (2016).

[18] Irzaman *et al.*, Characterization of optical and structural of lanthanum doped LiTaO3 thin films, *Integrated Ferroelect*. **167**, 141 (2015).

[19] X. Fan *et al.*, Band gap opening of graphene by doping small boron nitride domains, *J. Nanoscale*. **4** (6), 2157 (2012). DOI: 10.1039/c2nr11728b.

[20] J. Fraden, *Handbook of Modern Sensors*. 4th ed. (San Diego, CA: Springer Publishing, 2003).